

# Rotational Orientation of Transmembrane $\alpha$ -helices in Bacteriorhodopsin

## A Neutron Diffraction Study

Fadel A. Samatey<sup>1,4</sup>, Giuseppe Zaccai<sup>1</sup>, Donald M. Engelman<sup>2</sup>  
Catherine Etchebest<sup>3</sup> and Jean-Luc Popot<sup>4</sup>

<sup>1</sup>*Institut Laue-Langevin, BP 156X, avenue des Martyrs  
F-38042 Grenoble, France*

<sup>2</sup>*Yale University, Department of Molecular Biophysics and Biochemistry  
New Haven, CT 06511, U.S.A.*

<sup>3</sup>*Service de Biochimie Théorique and* <sup>4</sup>*Service de Photosynthèse  
Institut de Biologie Physico-Chimique, 13 rue Pierre et Marie Curie  
F-75005 Paris, France*

The rotational orientation of the seven transmembrane  $\alpha$ -helices (A-G) in bacteriorhodopsin has been investigated by neutron diffraction. The current model of bacteriorhodopsin is based on an electron density map obtained by high-resolution electron microscopy (EM). Assigning helix rotational positions in the EM model depended on fitting large side-chains, mainly aromatic residues, into bulges in the electron density map. For helix D, which contains no aromatic residues, the EM map is more difficult to interpret. For helices A and B, whose position and orientation had been determined previously by neutron diffraction, the positions defined by EM agree within experimental error with these earlier conclusions.

The orientation of all seven helices has been examined by using neutron diffraction on bacteriorhodopsin samples with specifically deuterated valine, leucine and tryptophan residues. Experimental peak intensities were compared to those predicted for an extensive set of structural models. The models were generated by (1) rotating all helices around their axis; (2) moving deuterated residues in the extramembrane loops about their probable positions and changing the weight of their contribution to the neutron diffraction pattern; (3) allowing deuterated side-chains to change their conformation. The analysis confirmed exactly the positions previously determined for helices A and B. For an optimal fit to the data to be obtained, the other five helices, including helix D, must lie either at or within 20° of their position in the current EM model. The complementarity of medium-resolution EM, neutron diffraction and model building for the structural study of integral membrane proteins is discussed.

**Keywords:** bacteriorhodopsin; membrane proteins; transmembrane  $\alpha$ -helix; neutron crystallography

### 1. Introduction

Purple membrane (PM $\dagger$ ) is a part of the plasma membrane of *Halobacterium salinarium* (formerly *H. halobium*), a bacterium that lives in high salt concentrations (Stoeckenius & Rowen, 1967; Oesterhelt & Stoeckenius, 1971). PM is composed of lipids (25% w/w) and a single integral membrane

protein, bacteriorhodopsin (BR; 75% w/w). Upon illumination, BR pumps protons from the cytoplasm to the extracellular medium (Oesterhelt & Stoeckenius, 1973). The energy transduction is effected by a retinal molecule covalently linked to a lysine residue on BR as a Schiff base.

The simple composition of PM, the interest in its function, its easy availability, and the highly ordered two-dimensional lattice that BR forms in the plane of the membrane have stimulated experiments aimed at determining the structure of the protein and the chemical mechanism of its function. In the years following the discovery of PM,

$\dagger$  Abbreviations used: PM, purple membrane; BR, bacteriorhodopsin; EM, electron microscopy; LW1, LW2, LW3, VAL, the four experimental samples used in the present study (see Materials & Methods).

X-ray diffraction (Blaurock & Stoeckenius, 1971; Blaurock, 1975; Henderson, 1975), electron crystallography (Unwin & Henderson, 1975; Henderson & Unwin, 1975), and neutron diffraction (Zaccaï & Gilmore, 1979) have been used to determine the arrangement of protein, lipids and water in the unit cell and the topology and secondary structure of the protein. Other biophysical, biochemical and genetic approaches have led, in particular, to defining the various steps of the proton-pumping cycle, establishing the sequence of BR, and identifying, by site-directed mutagenesis, residues that are important for proton translocation (reviewed by Khorana, 1988; Oesterhelt *et al.*, 1991).

An early low-resolution structure of BR, obtained by the combination of electron microscopy (EM) and electron diffraction, revealed the existence of seven transmembrane  $\alpha$ -helices, indexed 1 to 7, whose sequence and connectivity, however, could not be determined (Unwin & Henderson, 1975; Henderson & Unwin, 1975). The primary structure of BR (Ovchinnikov *et al.*, 1979; Khorana *et al.*, 1979) suggested that seven hydrophobic sequence segments, lettered A to G following their order in the sequence, were likely to form the transmembrane helices (Ovchinnikov *et al.*, 1979; Engelman *et al.*, 1980). A model was put forward for the three-dimensional folding of the polypeptide (Engelman *et al.*, 1980). There was little experimental evidence, however, as to which of the seven hydrophobic sequence segments (A to G) corresponded to each of the seven helices (1 to 7) found in the low-resolution structure, and therefore little information about the arrangement in space of the transmembrane residues involved in proton pumping. Neutron diffraction experiments using specific deuterium labeling were undertaken in order to try and solve this problem (Engelman & Zaccaï, 1980). Restricting labeling to specific hydrophobic segments was achieved by reconstituting renatured, crystalline PM from two proteolytic BR fragments originating from preparations with different isotopic compositions (Popot *et al.*, 1986, 1987). Neutron diffraction data were collected on labeled and control reconstituted samples and analyzed both by calculating difference Fourier maps and by a model building procedure. The two approaches agreed in locating segments A and B in positions 1 and 7 of the electron density map, respectively; the angular orientation of the two helices around their axis was determined using the model building approach (Popot *et al.*, 1989). In separate experiments, the position of deuterated retinal in the projection of the structure on the membrane plane was also established by neutron diffraction (Jubb *et al.*, 1984; Seiff *et al.*, 1986; Heyn *et al.*, 1988).

The best current model of BR has been built into a three-dimensional electron density map obtained by the combination of EM and electron diffraction (Henderson *et al.*, 1990). The resolution of the map is 3.5 Å in the membrane plane and about 10 Å perpendicular to it. Bulky features in the map were attributed to the ring of the retinal, in agreement

with the neutron diffraction location, and to aromatic side-chains. Comparison with sequence data permitted the identity and orientation of all seven transmembrane helices to be established. The location and orientation of helices A and B in the EM model agree exactly with those found previously by neutron diffraction (Popot *et al.*, 1989).

Helix D does not contain aromatic residues and there is no information on its orientation from previous neutron diffraction experiments. Its orientation in the EM model is essentially based on functional considerations and is the least certain (Henderson *et al.*, 1990). Helix D is located close to the retinal ring, and contains residue Asp115, which plays a poorly understood role in proton pumping (Mogi *et al.*, 1988; Stern *et al.*, 1989; Marinetti *et al.*, 1989).

In the present work, we have set out to define the rotational orientation of helix D in more detail by neutron diffraction, while, at the same time, gaining independent information on the rotational orientations of helices C, E, F and G. The neutron diffraction patterns of four BR samples were analyzed. Sample LW1 contained hybrid BR molecules in which chymotryptic fragment C-2 (residues 1 to 71, containing helices A and B) had all the non-exchangeable H atoms of leucines and the two H atoms on the C <sup>$\beta$</sup>  of tryptophans replaced by <sup>2</sup>H. Sample LW2, also with hybrid BR, was labeled in the same way in the complementary fragment C-1 (containing helices C to G). Sample LW3 was identical to LW2 except that deuterated C-1 has been isotopically diluted with unlabeled C-1 prior to renaturation. Sample VAL was a native PM sample in which the non-exchangeable H atoms of all valine residues were replaced biosynthetically by <sup>2</sup>H. Neutron diffraction data were analyzed using a model building approach that explores the rotational position of each of the seven helices while taking into account the uncertainty about the exact position of labeled residues located in the extra-membrane loops and the absence of information on the conformation adopted by amino acid side-chains in the protein.

## 2. Materials and Methods

### (a) Sample preparation

Culture of *Halobacterium salinarium* and extraction of PM followed Stoeckenius & Kunau (1968). For sample VAL, the valine in our defined culture medium, M1, was replaced by uniformly deuterated valine (CEA, France). The composition of M1 for 1 l of solution was as follows: NaCl 4.2 M, MgSO<sub>4</sub> 80 mM, KCl 27 mM, FeSO<sub>4</sub> 0.7 mM, CaCl<sub>2</sub> 2.3 mM, KH<sub>2</sub>PO<sub>4</sub> 1.5 mM, NH<sub>4</sub>Cl 9 mM, Na<sub>3</sub>C<sub>6</sub>H<sub>5</sub>O<sub>7</sub> (trisodium citrate) 10 mM, L-alanine 67 mM, L-arginine 32 mM, L-aspartic acid 60 mM, L-cystine 2 mM, L-glutamic acid 61 mM, glycine 80 mM, L-histidine 13 mM, L-isoleucine 23 mM, L-leucine 45 mM, L-lysine 48 mM, L-methionine 13 mM, L-phenylalanine 18 mM, L-proline 60 mM, L-serine 24 mM, L-threonine 25 mM, L-tryptophan 2 mM, L-tyrosine 14 mM, deuterated L-valine 34 mM, guanine 0.2 mM, cytosine 0.2 mM, uracyl

**Table 1**  
Distribution of deuterated positions in the four samples used in the present study

	VAL	LW1	LW2,LW3
helix A	7	58	
loop A-B	7		
helix B	7	36	
loop B-C	7	9	
helix C			76
loop C-D	7		
helix D	14		36
loop D-E	14		
helix E	7		31
loop E-F			
helix F	49		31
loop F-G	7		9
helix G	21		54

0.2 mM, thymine 0.2 mM; the pH was adjusted to 7.5 with NaOH. There was no difference in growth rate (judging from the increase of  $A_{640}$ ) between M1 and the medium containing peptone described by Stoekenius and Kunau (1968) (Samatey, 1992). The VAL sample used in the present work contained 300 mg of PM.

Hybrid samples were deuterated either on the leucine and tryptophan residues of fragment C-2 (residues 1 to 71; sample LW1) or on the leucine and tryptophan residues of fragment C-1 (residues 72 to 248; samples LW2 and LW3). Samples LW2 and LW3 were deuterated on the same positions, but the level of deuteration in sample LW3 was lowered, by dilution with unlabeled C-1 before renaturation, to 1/3 that in LW2. The preparation, characterization and diffraction patterns of these samples have been described by Popot *et al.* (1989) under the sample names #654, #655 and #660, respectively.

Deuteration in all labeled samples was introduced biosynthetically. For leucine, tryptophan and valine, this results in the back exchange of the deuterium on the C<sup>α</sup> (Sobol *et al.*, 1992). The aromatic deuterons of tryptophan are also exchanged back to hydrogen during the purification of fragments C-1 and C-2 (Popot *et al.*, 1989). As a result, deuteration in the final samples is carried by the C<sup>β</sup> of the tryptophans, the C<sup>β</sup>, C<sup>γ</sup>, C<sup>δ1</sup> and C<sup>δ2</sup> of the leucines and the C<sup>β</sup>, C<sup>γ1</sup>, and C<sup>γ2</sup> of the valines. The distribution of deuterated positions in the three samples used in the present study is summarized in Table 1.

#### (b) Determination of the extent of deuteration

The level of deuteration in sample VAL was measured by mass spectrometry in collaboration with O. Sorokine and A. van Dorssaeler at the Ecole Supérieure de Chimie (Strasbourg-France), as described by Schindler *et al.* (1993). The mass of delipidated bacteriorhodopsin was determined with an accuracy of  $\pm 8$  Da for sample VAL and for a control, unlabeled sample. A deuteration level of  $70 \pm 8\%$  was calculated from the mass difference. Absence of spillover of labeling into other classes of amino acids (Trehwella *et al.*, 1983) was controlled by using [<sup>3</sup>H]-valine. An analysis of the radioactivity of the 20 residues purified from a culture of *Halobacterium salinarium* grown on [<sup>3</sup>H]-valine in medium M1 showed that there was no radioactivity above background elsewhere than in the valine fraction.

The extent of deuteration in samples LW1 to 3 could not be determined precisely (see Popot *et al.*, 1989). However, we have shown previously that even large

uncertainties in the level of deuteration assumed for the calculation have negligible effects on the ranking of the models (Popot *et al.*, 1989). In the present work, calculations on LW1 data assumed a deuteration level of 60%, in order to permit direct comparison of the  $\chi^2_v$  values with the results of Popot *et al.* (1989). For samples LW2 and LW3, we assumed deuteration levels of 70% and 30%, respectively, which gave slightly better  $\chi^2_v$  values without changing the ranking of the models.

#### (c) Data collection and reduction

Sample VAL, collected as a PM suspension in H<sub>2</sub>O, was dried on quartz slides and allowed to reach equilibrium for more than 24 hours in 100% relative humidity in an air-tight sample holder at 25°C. Neutron diffraction data were collected on the D16 diffractometer at the Institut Laue Langevin in Grenoble. The design of the diffractometer and the treatment of the diffraction patterns were similar to those described by Zaccari and co-workers (Jubb *et al.*, 1984). The neutron beam wavelength  $\lambda$ , selected by a graphite monochromator, was 4.54 Å with a dispersion  $\Delta\lambda/\lambda \approx 1\%$ . The neutron beam was collimated by 3 sets of cadmium slits. Other experimental conditions and data reduction were as described by Popot *et al.* (1989). As compared with data collected previously on PM samples deuterated on valine residues (Trehwella *et al.*, 1983), the VAL data differ with respect to (1) a higher accuracy on the weakest reflections, (2) a procedure for separating overlapping reflections that is more consistent with other data sets used in this study. Diffraction data on samples LW1, LW2 and LW3 and on a control (reconstituted) sample (#267) are taken from Popot *et al.* (1989). The diffraction intensities of all samples used in this study are listed in Table 2.

#### (d) Analysis

The analysis was done by comparing the experimental neutron diffraction intensities to intensities calculated from different BR models, as described previously (Popot *et al.*, 1989). As compared with the earlier work, model building incorporated recent crystallographic progress achieved by Henderson *et al.* (1990) and examined the possible impact of further sources of uncertainty.

##### (i) Model building

Atomic models of BR were generated by (i) rotating helices around their axes; (ii) moving deuterated residues in the extramembrane loops about their probable positions and changing the weight of their contribution to the neutron diffraction pattern; (iii) allowing deuterated side-chains to adopt various conformations.

##### (i)(a) Helix rotations

The starting structure was the EM model of Henderson *et al.* (1990) (the erroneous Ile111 in the coordinates was replaced with a leucine). Helix axes were determined using the program PCURVE (Sklenar *et al.*, 1989). For each helix, 18 sets of coordinates were generated, each corresponding to a rotation of  $N \times 20^\circ$  about the helix axis, with  $N$  an integer varying from 0 to 17. Rotation angles are measured clockwise looking from the helix N terminus, the initial position ( $N=0$ ) being the position defined by the EM model. Any rotation of one of the seven helices generates a new rotational model to be tested. Following equation (1) (see below), only the coordinates of the labeled residues had to be calculated for each model.

**Table 2**  
*Normalized, Lorentz-corrected intensities for the control sample and for labeled samples*

(h,k) indices	Control	VAL	LW1	LW2	LW3	Standard deviations ( $\sigma_o$ )
1,1	37,006	39,449	39,996	65,211	47,570	5
2,0	13,480	11,941	14,087	30,243	17,658	7
2,1	8456	16,646	12,808	4925	7533	8
3,0	977	702	2391	1184	1650	38
2,2	7504	10,111	11,917	8844	9565	14
3,1	8458	14,313	5317	9974	8829	14
4,0	5050	5474	4274	8635	6992	4
3,2	5898	6121	6240	2044	5102	8
4,1	12,452	12,071	10,868	7542	10,204	11
5,0	7301	4589	6548	1720	4925	7
4,2	11,148	7018	12,148	5606	8589	6
5,1	4476	4676	5695	2537	3115	14
4,3	33,747	26,435	30,320	16,170	26,646	3
5,2	7096	5675	6375	3896	7276	33
6,1	3674	5989	1866	3319	3780	14
7,0	8430	6810	7024	5454	6957	13
6,2	2020	1555	1205	2506	1340	71
7,1	5386	4088	3477	2749	4827	25

The VAL data are from the present work. Other data, including average relative standard deviations, are from Popot *et al.* (1989), where LW1, LW2, LW3 were described as samples #654, #655 and #660, respectively.

(i)(b) *Labeled residues in the loops*

Labeled residues in the extramembrane loops (i.e. outside the 7 transmembrane helices) also contribute to the diffraction pattern. The unpublished, provisional, coordinates for the BR loops were kindly communicated to us by Richard Henderson (MRC, Cambridge). They are not as reliable as those for the rest of the structure (R. Henderson, private communication). We took this uncertainty into account by moving these residues on an XY grid in the plane of the membrane. Both X and Y coordinates were changed by  $\pm 4 \text{ \AA}$  about their initial position in 2  $\text{\AA}$  steps, resulting in 25 different positions for each loop residue. In the calculation of predicted structure factors, the contribution of loop residues could be cancelled by giving them a SCALE factor equal to zero.

(i)(c) *Side-chain conformations*

The exact position of deuterons in leucine and valine residues depends on the conformation of their side-chains. In order to test whether assigning arbitrary conformations to labeled side-chains could be a source of systematic errors, models were built with different side-chain rotamers shown to predominate in well-resolved protein structures (Tuffery *et al.*, 1991).

(ii) *Calculation of model intensities*

Calculation of model intensities was done as described previously (Popot *et al.*, 1989). The diffraction intensity  $I_{c,i}$  of the *i*th diffraction peak predicted by any given model is given by:

$$I_{c,i} = (F_{D,i})^2 = [F_{N,i} + (F_{L,i} \times \text{SCALE})]^2 \quad (1)$$

where  $F_{D,i}$  is the calculated structure factor of reflection *i* of the deuterated sample;  $F_{N,i}$  is the experimental structure factor of the native sample for the same reflection;  $F_{L,i}$  is the calculated structure factor for the label (difference between deuterium and hydrogen); SCALE is a constant corresponding to the deuteration level of the labeled sample. Because of the expression for  $I_{c,i}$ , the only difference between different models arises from the posi-

tions of the deuterated residues. Observed and calculated intensities were normalized to the same sum.

(iii) *Ranking of the models*

Ranking of the models was done through the calculation of a  $\chi^2$  factor, as described previously (Popot *et al.*, 1989):

$$\chi^2 = \sum_{i=1}^N \frac{(I_{c,i} - I_{o,i})^2}{\sigma_{c,i}^2 + \sigma_{o,i}^2} \quad (2)$$

$I_c$  and  $I_o$  are the calculated and observed intensities, respectively;  $\sigma_c$  and  $\sigma_o$  are the respective errors on these intensities. For samples VAL, LW1 and LW3, the sum was usually taken over all the (h,k) diffraction peaks. For sample LW2, we noted that the relatively high values of  $\chi^2$  were due in part to reflections (1,1) and (2,0), which were systematically higher in the observed pattern than in calculated ones. Because these reflections correspond to very low resolution data, they are essentially model-insensitive. This was checked by repeating  $\chi^2$  calculations while omitting these two reflections;  $\chi^2$  values decreased, but the ranking order of the models remained the same. In all cases,  $v$  was taken as equal to  $N$ , the total number of reflections taken into account. Note that, because moving loop residues and changing side-chain conformations increases the number of adjustable parameters, the  $\chi^2$  value associated with any given rotational model is expected to diminish whenever these parameters are taken into account, whether the rotational model is correct or not.

Sources of errors in the experimental intensities and in the different steps of the calculation of theoretical intensities have been discussed by Popot *et al.* (1989).

### 3. Results

#### (a) *Overall strategy*

BR models were ranked by comparing predicted reflection intensities calculated for each model to

experimental intensities using a  $\chi_v^2$  test (see Materials and Methods). Models that fit the data better yield lower  $\chi_v^2$  values. Models differed by the rotational orientation assigned to each helix, by the position assigned to each loop residue and by the conformation assigned to each deuterated side-chain. The combination of these assignments generates enormous numbers of models ( $>10^{11}$  for sample LW1,  $>10^{26}$  for samples LW2 and LW3 and  $>10^{18}$  for sample VAL), which cannot be analyzed exhaustively. A step-wise screening procedure was therefore adopted. It was first tested on the data from sample LW1 (labeled in helices A and B). These data had been analyzed previously by Popot *et al.* (1989), using a simpler procedure that did not take into account the possible effect of moving loop labels or assigning different side-chain conformations. We then analyzed the rotational orientations of helices C to G using the data from samples LW2, LW3 and VAL.

#### (b) Helices A and B

In sample LW1, labeling was restricted to helices A and B (comprising a total of ten leucine and two tryptophan residues) and a single loop residue (Leu66). The model building method generates more than  $10^{11}$  models ( $18^2$  rotational models  $\times$  25 positions for Leu66  $\times$   $6^{10}$  combinations of conformations). The best combinations of rotational orientations for helices A and B were first determined (out of  $18^2 = 324$  models), without taking into account side-chain conformations or the contribution of Leu66. The effect of displacing Leu66 and of varying the side-chain conformations of the transmembrane leucine residues was then investigated.

The first step (rotations in  $20^\circ$  steps without inclusion of the loop residue) was similar to the previous analysis of the same data by Popot *et al.* (1989), and yielded comparable  $\chi_v^2$  values. The best of the 324 models had helix A in its EM position and helix B within  $\pm 20^\circ$  from it (not shown). In a second step, we examined the influence of the loop residue on the ranking of the rotational models. Including Leu66 in the analysis increased  $\chi_v^2$  values, suggesting that giving it the same weight as that of the other leucines may be an overestimate. Twenty-five variants of each rotational model were built by displacing Leu66 in 2 Å steps on a square  $4 \text{ Å} \times 4 \text{ Å}$  grid centered on its EM position, yielding a total of 8100 models. The hierarchy of the best models remained the same as when Leu66 was not taken into account (not shown). Best  $\chi_v^2$  values were obtained when Leu66 was moved at the border of our field of exploration, 5.6 Å away from its EM position in the direction of helix C. The position of Leu66 suggested by this analysis is far from certain, however, given that (1) displacing Leu66 has less influence on  $\chi_v^2$  values than optimizing side-chain conformations (see below); (2) it is not known whether Leu66 is as well ordered as helix leucines and contributes as much to the diffraction pattern; (3) we did not attempt to explore whether a better

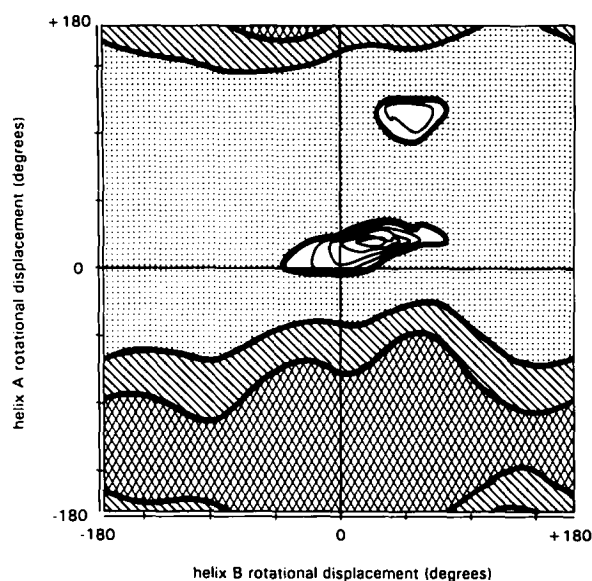


**Figure 1.** Rotational position of helices A and B. Contour plot showing the variation of  $\chi_v^2$  as a function of the rotational position of helices A and B. Sample LW1. Leucines were given their most frequent conformation. The single extramembrane leucine, Leu66, in the loop connecting helices B and C, was set in its optimal position (see the text). All reflections were taken into account in the calculation. Cross-hatched region,  $\chi_v^2 > 7.5$ ; hatched region,  $5.0 < \chi_v^2 < 7.5$ ; dotted region,  $1.5 < \chi_v^2 < 5.0$ ; white regions, contour curves spaced 0.1 apart from  $\chi_v^2 = 1.4$  to  $\chi_v^2 = 1.1$ .

fit to the data could be obtained by moving Leu66 still further from its initial position. When Leu66 was set in its optimal position, the best four of the 324 rotational models had helices A and B at or within  $20^\circ$  from their EM position (Figure 1).

In a last step, the effect of side-chain conformation on the ranking of the best rotational models was examined. Because of limitations on computing time, the analysis had to be restricted to a selection of rotational models. In a first trial, helix rotations were limited to  $\pm 20^\circ$ . Leu66 was moved over its 25 positions, and helix leucines were allowed to adopt either of the two most frequent conformations (which, taken together, represent 71% of leucine residues in well-resolved structures; see Tufféry *et al.*, 1991). Optimizing side-chain conformations of course resulted in better values of  $\chi_v^2$ , but the hierarchy of rotational models and the optimal position for Leu66 were not affected (not shown). In a second trial, helix rotations were limited to  $\pm 80^\circ$ . Leu66 was left in its optimal position and helix leucines were allowed to take any of their three most probable side-chain conformations ( $9 \times 3^{10} \approx 5.3 \times 10^5$  models). Differences between models diminished (because the prediction from an incorrect model can be partially improved by moving the side-chains in a compensatory manner), but the hierarchy given by the rotational analysis alone was maintained. The best model still had helices A and B in their initial positions (Table 3).

**Table 3**  
 Values of  $\chi_v^2$  for 25 combinations of rotational positions of helices A and B

Helix B	Helix A	-40°	-20°	0°	+20°	+40°
-40°		1.84	1.14	0.90	1.13	2.08
-20°		1.94	1.15	0.84	0.92	1.78
0°		1.93	1.20	<b>0.80</b>	0.85	1.52
+20°		2.24	1.39	0.86	0.86	1.37
+40°		2.87	1.67	1.02	0.90	1.25

Data from sample LW1. Leucine side chains were left free to adopt any of their 3 most frequent conformations. Leu66 was left in its optimal position. All reflections were taken into account in the calculation of  $\chi_v^2$ . Calculations were actually performed over  $\pm 80^\circ$  for both helices, in order to check that the true minimum had not been missed. Only the central part of the resulting table is shown here.

These observations indicate that analyzing helix orientation while keeping arbitrary settings for loop labels and conformers does not induce strong bias in the hierarchy of rotational models. The quality of the fit to the data, however, is sensitive to the position of loop residues and to the choice of conformers.

(c) *Helices C, D, E, F and G*

In the analysis of the last five helices, the same strategy as the one tested on helices A and B was followed, with some simplifications made necessary by the greater combinatorial complexity. Samples LW2, LW3 and VAL were used in parallel. In samples LW2 and LW3, helices A and B contained no label and did not need to be taken into account when calculating predicted diffraction patterns. In sample VAL, valine residues in helix A, helix B and in the loops connecting A to B and B to C were deuterated to the same extent as those in the rest of the structure. They were taken into account in the same way as the other valine residues, but the rotational position of helices A and B was set to  $0^\circ$  in all calculations. All helices contain at least three leucines and there is a single leucine (Leu201) in the loops, while helix C has no valine, helix E has a single one, and six out of the 21 valines are located in the loops (Table 1).

In the first step of the analysis, approximate orientations were determined for each of the five helices C to G individually. The labeled residues located in the loops were left in their EM positions and leucine and valine residues were placed in their most probable conformations. Each helix in turn was set successively in each of its 18 possible angular positions. The other four helices were left free to rotate in  $20^\circ$  steps over  $\pm 60^\circ$  around their EM position, yielding  $7^4 = 2401$  rotational models for each orientation of the helix under study. The lowest  $\chi_v^2$  obtained for each orientation is indicated in Figures 2 and 3. Similar results were obtained

when the rotation range was extended to  $\pm 80^\circ$  (not shown).

For all helices except helix C, all models giving good fits to the LW2, LW3 and VAL data sets corresponded to positions in the vicinity of the EM position. In one case (helix D), an ambiguity left by the analysis of the LW samples could be removed by consideration of VAL data. For helix E, the most poorly labeled, data were more ambiguous and a wide range of positions was considered for further analysis. For helix C, best fits to the LW2 and LW3 data sets were obtained for two positions around  $-160^\circ$  and  $-20^\circ$  (Figure 2). This ambiguity may arise because of the roughly symmetric distribution of deuterons around the axis of the helix (see Figure 1 in Popot *et al.*, 1989). It cannot be resolved using

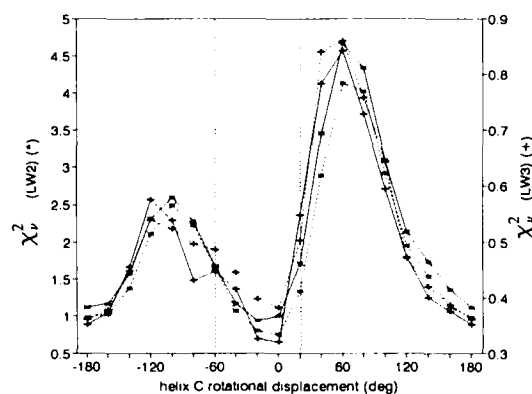
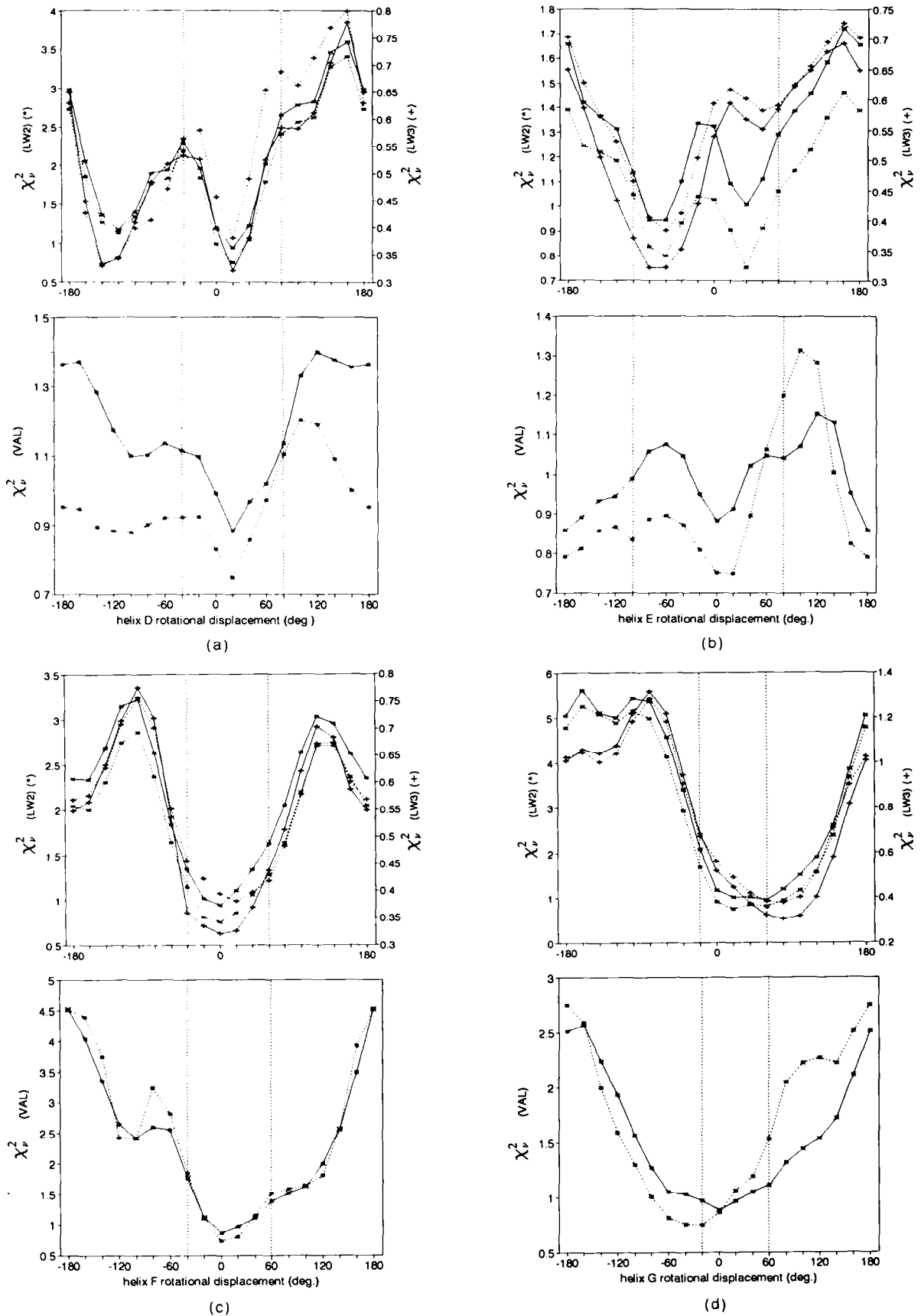


**Figure 2.** Determination of a restricted range of rotational positions for helix C. Data from samples LW2 and LW3. For each of the 18 positions of helix C, the  $\chi_v^2$  value indicated is the best that can be obtained while leaving helices D, E, F and G free to rotate by up to  $\pm 60^\circ$  from their EM position. Leucine side-chains were left in their most frequent conformation. Leu201 was either left in its EM position (-\*- -, -+ -), or not included in the calculations (--\*- -, --+ -). Left scale: data from LW2 (--\*- -, -\*- -); right scale: data from LW3 (--+ - -, -+ - -). Vertical lines delimit the restricted rotational domain selected for subsequent calculations.

**Figure 3.** Determination of restricted ranges of rotational positions for helices D to G. Data from samples LW2, LW3 and VAL. (a), helix D; (b), helix E; (c), helix F; (d), helix G. For each of the 18 positions of the helix under study, the  $\chi_v^2$  value indicated is the best that can be obtained while leaving the other four helices free to rotate by up to  $\pm 60^\circ$  from their EM positions. Leucine and valine side-chains were left in their most frequent conformation. In the analysis of



samples LW2 and LW3 (top part of each panel). Leu201 was either left in its EM position (—\*—, —+—) or not included in the calculations (---, ---). Left scale: data from LW2 (---, —\*—); right scale: data from LW3 (---, —+—). In the analysis of sample VAL (bottom), helices A and B were left in their EM position; loop valines were either left in their EM position (—\*—), or not included in the calculations (---). Throughout the figure, vertical lines delimit the restricted rotational domains selected for subsequent calculations.

the VAL data, since helix C contains no valine. However, a position around  $-160^\circ$  is incompatible with the lateral amphipathy of the helix (as well as with functional data) and was considered no further.

The analysis summarized in Figures 2 and 3 defines for each helix a domain outside which an optimal fit to the data is unlikely to be found (delimited by vertical lines in Figures 2 and 3). In a second step of the analysis, helices C to G were left free to take any combination of rotational positions within these angular limits, generating 10,500 distinct rotational models. Among those, only 33 were found to fit each of the three sets of experimental data as well as or better than the EM model. Of these models, 23 were redundant, in the sense that they could be converted to another of the 33 models by rotating a single helix by  $20^\circ$ , thereby improving the quality of the fit to the data. The remaining ten best models are listed in Table 4 in the approximate order of decreasing overall fit. In all of them, all five helices under consideration occupy positions at most at  $40^\circ$  and generally within  $20^\circ$  from their EM position.

In a finer analysis, 7200 models in the angular domains described above were examined once again using the VAL and LW2 data, this time taking into account the effects of moving around the deuterated leucines and valines located in the loops and changing the conformation of deuterated valine side-chains among their three most probable conformers. As had been the case with helices A and B, there was no difference in the final ranking of rotational models even though better values of  $\chi_v^2$  were obtained for certain loop and side-chain configurations (not shown).

For all helices, the most frequently observed posi-

tion is identical to that in the EM model, or at most  $20^\circ$  away from it. For helices C, E, F and G, rotational positions are accurately determined by the EM data. The  $20^\circ$  variations about the EM model positions found for these four helices represent the limits of accuracy of the neutron diffraction approach. For the determination of the position of helix D, models therefore were further constrained by leaving helices C, E, F and G in their EM position, while helix D was moved through  $360^\circ$  (Figure 4). Loop residues either were left in their EM position or were not included in the calculations. Deuterated side-chains were set in their most frequent conformation. Best fits to the data were obtained with D at  $0^\circ$  to  $+20^\circ$  (samples LW2 and LW3) or  $+20^\circ$  to  $+40^\circ$  (sample VAL). While a position at  $+20^\circ$  would represent the best compromise between the three sets of neutron diffraction data, the  $0^\circ$  one is most compatible with the results of helix packing calculations (Tufféry *et al.*, 1994).

#### 4. Discussion

##### (a) Accuracy of helix rotational positions

The strategy followed in the present work is similar to that which previously led to determining the position and rotational orientation of helices A and B (Popot *et al.*, 1989). Significant methodological improvements are (1) starting from a more accurate model (Henderson *et al.*, 1990); (2) using data from samples with different labels; (3) including in the analysis the contribution of labeled residues in the loops and (4) including the effect of varying side-chain conformations. Moving loop residues and optimizing side-chain conformers increases the number of parameters in the fit, which

**Table 4**  
The 10 best rotational models for helices C to G

Helix C	Helix D	Helix E	Helix F	Helix G	$\chi_v^2$ (VAL)	$\chi_v^2$ (LW2)	$\chi_v^2$ (LW3)
$-20^\circ$	$+20^\circ$	$+20^\circ$	$0^\circ$	$0^\circ$	0.91	1.56	0.74
$-20^\circ$	$+20^\circ$	$0^\circ$	$0^\circ$	$0^\circ$	0.88	2.27	0.62
$-20^\circ$	$+40^\circ$	$-20^\circ$	$0^\circ$	$+20^\circ$	1.08	2.06	0.57
$-40^\circ$	$+20^\circ$	$-20^\circ$	$0^\circ$	$0^\circ$	0.95	2.69	0.56
$0^\circ$	$+20^\circ$	$+20^\circ$	$0^\circ$	$0^\circ$	0.91	2.30	0.69
$-20^\circ$	$+20^\circ$	$0^\circ$	$+20^\circ$	$0^\circ$	1.04	2.60	0.61
$-40^\circ$	$+20^\circ$	$-40^\circ$	$0^\circ$	$0^\circ$	1.08	3.03	0.53
$+20^\circ$	$+20^\circ$	$+40^\circ$	$0^\circ$	$+20^\circ$	1.02	2.40	0.72
$0^\circ$	$+40^\circ$	$0^\circ$	$0^\circ$	$+20^\circ$	1.01	2.65	0.70
$-20^\circ$	$+60^\circ$	$-20^\circ$	$0^\circ$	$+20^\circ$	1.05	3.32	0.71
Range							
$-40^\circ$ to $+20^\circ$	$+20^\circ$ to $+60^\circ$	$-40^\circ$ to $+40^\circ$	$0^\circ$ to $+20^\circ$	$0^\circ$ to $+20^\circ$			
Most frequent position							
$-20^\circ$	$+20^\circ$	$-20^\circ/0^\circ$	$0^\circ$	$0^\circ$			
EM model (every helix at $0^\circ$ ):					1.09	3.44	0.74

$\chi_v^2$  values were calculated for each set of data with the following assumptions: VAL sample, most frequent valine conformation, loop residues in EM positions, helices A and B at  $0^\circ$ , all reflections taken into account; LW2 sample, most frequent leucine conformation, Leu201 in its EM position, reflections (1.1) and (2.0) excluded from the calculation of  $\chi_v^2$ ; LW3 sample, same as sample LW2 but reflections (1.1) and (2.0) included in the calculation of  $\chi_v^2$ . Following the 10 best models and their  $\chi_v^2$  values are given the range of positions occupied by each helix in these models, its most frequent position, and the  $\chi_v^2$  values obtained for the EM model.

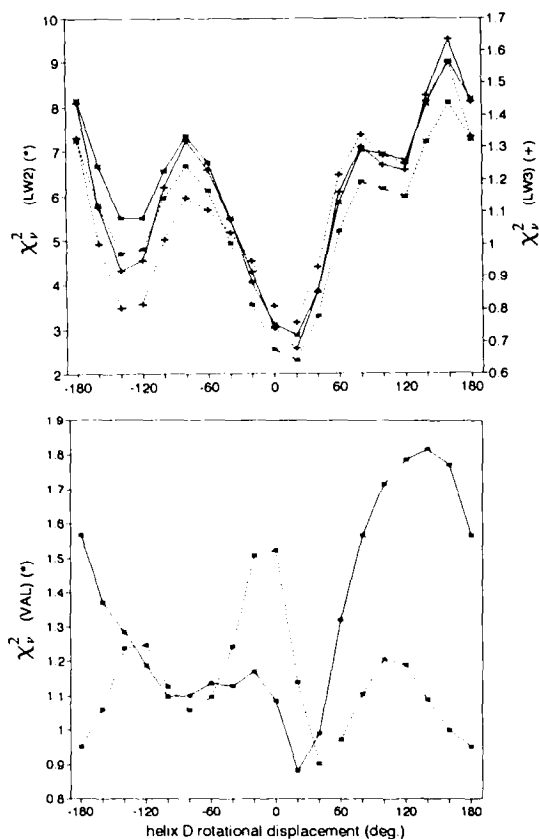


**Figure 4.** Determination of the rotational position of helix D assuming all other helices to be in their EM position. Same as Figure 3(a), except that all helices but helix D were set at  $0^\circ$ .

necessarily leads to lower  $\chi^2_v$  values. Because the ranking of models is not affected, it shows that the rotational search is not biased by inappropriate assumptions concerning these parameters. Since many models with different combinations of side-chain conformations are predicted to have indistinguishable diffraction patterns, the data cannot be used to specify the conformation of any particular side-chain. For the same reason, it is not possible to determine the exact location of the loop residues (except, possibly, for Leu66; see Results).

Our primary objective in undertaking this study was to establish the orientation of helix D, which is poorly defined in the electron density map. Because our labeling is not restricted to helix D, however, its position cannot be determined unless that of the other labeled residues is known. In practice, we have re-determined the orientation of all seven helices. Re-examination of helices A and B could be done independently from that of the other helices, because we had a specifically labeled sample. This analysis gave us an opportunity to check our methodology and to examine, on this simpler system, the effect of making simplifying assumptions about the position of loop residues and the conformation of side-chains.

The analysis of helices C to G had to be done simultaneously, which increased combinatorial problems. It offered, however, the opportunity to

estimate from a comparison of our positions for helices C, E, F and G with those given by Henderson and colleagues, the accuracy of our conclusions regarding the position of D. The main conclusion of the rotational search is that a good fit to the data is obtained when helices C to G are left in the position they adopt in the EM model. For most helices, there is a range of accessible positions, the most frequent of which lies either at or within  $20^\circ$  of the EM position, that gives at least as good a fit to the neutron diffraction data as the EM model does. This suggests that the limit of accuracy of our approach is probably about  $20^\circ$ . Rotating an  $\alpha$ -helix by  $20^\circ$  corresponds to a linear displacement of about  $1.5 \text{ \AA}$  of the C $^\alpha$  carbons of a valine or leucine side-chain. This accuracy is consistent with that expected from data collected at  $7 \text{ \AA}$  resolution (see below).

We conclude therefore that the orientation of helix D in the EM model, even though it was considered by Henderson *et al.* (1990) to be "the least certain part of (their) interpretation", is likely to be within  $20^\circ$  of the correct position. This conclusion is consistent with the result of a model building analysis of the packing of  $\alpha$ -helices in BR recently carried out (Tufféry *et al.*, 1994). The longitudinal position of helix D along its axis, on the other hand, needs to be slightly revised (R. Henderson, personal communication; Tufféry *et al.*, 1994). Helix D is almost exactly perpendicular to the membrane plane. Since we are using projection data, which do not contain any information on the longitudinal position of D, our model building analysis is not dependent on such displacements.

(b) *Concerning the use of neutron diffraction in the study of integral membrane proteins*

During the 15 years that separate the publication of the  $7 \text{ \AA}$  resolution EM structure of BR from that of the current model, a number of neutron diffraction experiments have been performed on purple membranes. A similar situation may arise again, namely, electron or X-ray crystallography yielding a medium-resolution structure of a membrane protein, the interpretation of which could be aided by neutron diffraction data. Two reasons for this belief are the well-known difficulty of obtaining very well-ordered 2D or 3D crystals of membrane proteins (see Michel, 1991; Reiss-Husson, 1992) and the technical problems associated with collecting high-resolution EM images (Henderson *et al.*, 1986). It is therefore of interest to examine what the contribution of neutron diffraction to the study of BR has been and whether it could also help in the study of other integral membrane proteins.

All based on deuterium labeling, neutron diffraction experiments on BR fall into two broad categories: (1) studies of function, where  $^1\text{H}_2\text{O}/^2\text{H}_2\text{O}$  exchange is used to examine the hydration of the membrane under different conditions (see e.g. Zaccai, 1987); (2) studies of particular structural features using specific deuterium labeling. Neutron

diffraction results continue to be irreplaceable for the first category of experiments. As an example of the second category of study, deuterated retinal has been located in projection by Jubb *et al.* (1984). This result was confirmed by Seiff *et al.* (1986) and Heyn *et al.* (1988), who took the study further by deuterating the two ends of the molecule separately, to show the way it was oriented. Experiments involving deuteration of specific amino acids, with or without reconstitution of BR from fragments, were aimed at identifying and orienting the helices in the 7 Å resolution structure (Engelman & Zaccari, 1980; Popot *et al.*, 1989). The present work probably explores the limits of this method. It is reasonable to believe that, in the absence of the high-resolution EM structure, our approach probably would have solved the arrangement of all of the seven helices. However, given the large number of free parameters (placing 5 helices over 5 positions without strong constraints on their orientations), and the relatively limited number of observables (18 useful reflections for each sample), removing ambiguities might have required the preparation of at least one other specifically labeled sample.

In all the analyses, use had to be made of a low-resolution EM structure, either for phasing the neutron diffraction reflections and/or as a starting point for building models. Except in the present paper, where the most recent EM model was used, the 7 Å resolution EM structure and the sequence were the only "outside" structural information required to interpret the neutron diffraction data. Conversely, knowledge of the location and orientation of the retinal molecule in projection, as well as that of the location and orientation of helices A and B, helped in the interpretation of the 3D EM map calculated at significantly higher resolution, and are in agreement with the final model (Henderson *et al.*, 1990). Perhaps the most important point to be emphasised is that, thanks to the combination of specific deuteration and neutron diffraction, low-resolution data can be interpreted to yield "higher resolution" information. This simply reflects the fact that, if contrast is high enough, the position of a label can be determined with high accuracy as the center of a peak of density (Plöhn & Büldt, 1986). X-ray or EM data at 7 Å-resolution cannot be interpreted in atomic detail, even on the basis of a model, because of the low contrast between the different components of a structure. This is overcome in neutron diffraction by deuterium labeling. The present study, as well as those focused on the location of the retinal, confirm that structural features can be determined to an accuracy of 1 to 2 Å using powder diffraction patterns collected out to 6.9 Å, with strong reflections extending only to 8.9 Å.

In cases where there is a good low-resolution structure, therefore, low-resolution neutron data combined with deuterium labeling is a very useful technique. This is particularly true for integral membrane proteins, whose transmembrane regions are often made up of bundles of  $\alpha$ -helices (see Popot

& Engelman, 1990; Popot, 1993; Popot *et al.*, 1993). Good approximations of the structure can be generated by combining  $\alpha$ -helices, considered as solid blocks easily built using ideal  $\alpha$ -helix parameters. Working with projection data limits the consequences of the usual uncertainty about the exact position of helix ends, since most helices are more or less normal to the membrane plane. Requirements for applying this approach to other systems than BR are, however, rather demanding. It is not possible to work on rare, selected 2D crystals as can be done with EM. Even though it is unnecessary for the whole preparation to be crystalline, crystals must comprise a large enough fraction of the samples (presumably tens of %) for reflection intensities to be measured accurately. Specific deuterium labeling can be achieved either biosynthetically, or by biochemical reconstitution, or, as was done by Popot *et al.* (1989) and in the present work, by combining both. Extensive deuteration is more easily obtained in prokaryotic organisms, which can grow in 100%  $^2\text{H}_2\text{O}$ , but this is not an absolute requirement: in the present work, accurate information was obtained from sample LW3, in which the level of deuteration had been lowered by dilution to  $\approx 25\%$ . Finally, and most demanding, the necessary amounts of crystalline deuterated material are considerable (of the order of tens of mg) if the time required for data collection is not to exceed days. This limit could be lowered by using brighter sources. The sample, of course, has to be stable for such durations.

### (c) Conclusion

In conclusion, independent examination by neutron diffraction of the rotational orientation of the seven transmembrane  $\alpha$ -helices in BR has yielded positions that are consistent with those in the current EM model, with an accuracy estimated at about  $20^\circ$ . In a parallel study, Tufféry *et al.* (1994) have developed a model building approach designed to explore possible rotational arrangements within bundles of transmembrane  $\alpha$ -helices with known axis positions. The results of the two studies are in very good agreement.

We would like to thank R. Henderson (MRC, Cambridge) for private communication of the provisional coordinates of loop residues; R. Lavery, P. Tufféry, D. Piazzola and R. Savinelli (IBPC, Paris) for help and advice about computers and programs; O. Sorokine and A. van Dorssaeler (Ecole de Chimie, Strasbourg) for the mass spectrometry measurements; J. Gagnon (IBS, Grenoble) for amino acid purification and analysis; and A. S. Arseniev (Shemyakin Institute, Moscow) for a discussion about biosynthetic deuteration of BR. This work was supported by a grant (MRT 87.C.0395) from the Ministère de la Recherche et de la Technologie to J.-L.P.

### References

- Blaurock, A. E. (1975). Bacteriorhodopsin: a transmembrane pump containing  $\alpha$ -helices. *J. Mol. Biol.* **93**, 139-158.

- Blaurock, A. E. & Stoerkenius, W. (1971). Structure of the purple membrane. *Nature New Biol.* **233**, 152–155.
- Engelman, D. M. & Zaccari, G. (1980). Bacteriorhodopsin is an inside-out protein. *Proc. Nat. Acad. Sci., U.S.A.* **77**, 5894–5898.
- Engelman, D. M., Henderson, R., McLachlan, A. D. & Wallace, B. A. (1980). Path of the polypeptide in bacteriorhodopsin. *Proc. Nat. Acad. Sci., U.S.A.* **77**, 2023–2027.
- Henderson, R. (1975). Structure of the purple membrane from *Halobacterium halobium*: analysis of the X-ray diffraction pattern. *J. Mol. Biol.* **93**, 123–138.
- Henderson, R. & Unwin, P. N. T. (1975). Three-dimensional model of purple membrane obtained by electron microscopy. *Nature (London)*, **257**, 28–32.
- Henderson, R., Baldwin, J. M., Downing, K. H., Lepault, J. & Zemlin, F. (1986). Structure of purple membrane from *Halobacterium halobium*: recording, measurement and evaluation of electron micrographs at 3.5 Å resolution. *Ultramicroscopy*, **19**, 147–178.
- Henderson, R., Baldwin, J. M., Ceska, T. A., Zemlin, F., Beckmann, E. & Downing, K. H. (1990). Model for the structure of bacteriorhodopsin based on high resolution electron cryo-microscopy. *J. Mol. Biol.* **213**, 899–929.
- Heyn, M. P., Westerhausen, J., Wallat, I. & Seiff, F. (1988). High-sensitivity neutron diffraction of membranes: location of the Schiff base end of the chromophore in bacteriorhodopsin. *Proc. Nat. Acad. Sci., U.S.A.* **85**, 2146–2150.
- Jubb, J. S., Worcester, D. L., Crespi, H. L. & Zaccari, G. (1984). Retinal location in purple membrane of *Halobacterium halobium*: a neutron diffraction study of membranes labeled *in vivo* with deuterated retinal. *EMBO J.* **3**, 1455–1461.
- Khorana, H. G. (1988). Bacteriorhodopsin, a membrane protein that uses light to translocate protons. *J. Biol. Chem.* **263**, 7439–7442.
- Khorana, H. G., Gerber, G. E., Herlihy, W. C., Gray, C. P., Anderegg, R. J., Nihel, K. & Biemann, K. (1979). Amino acid sequence of bacteriorhodopsin. *Proc. Nat. Acad. Sci., U.S.A.* **76**, 5046–5050.
- Marinetti, T., Subramaniam, S., Mogi, T., Marti, T. & Khorana, H. G. (1989). Replacement of aspartic residues 85, 96, 115, or 212 affects the quantum yield and kinetics of proton release and uptake by bacteriorhodopsin. *Proc. Nat. Acad. Sci., U.S.A.* **86**, 529–533.
- Michel, H. (ed.) (1991). *Crystallization of membrane proteins*. CRC Press, Boca Raton.
- Mogi, T., Stern, L. J., Marti, T., Chao, B. H. & Khorana, H. G. (1988). Aspartic acid substitutions affect proton translocation by bacteriorhodopsin. *Proc. Nat. Acad. Sci., U.S.A.* **85**, 4148–4152.
- Oesterhelt, D. & Stoerkenius, W. (1971). Rhodopsin-like protein from the purple membrane of *Halobacterium halobium*. *Nature New Biol.* **233**, 149–152.
- Oesterhelt, D. & Stoerkenius, W. (1973). Functions of a new photoreceptor membrane. *Proc. Nat. Acad. Sci., U.S.A.* **70**, 2853–2857.
- Oesterhelt, D., Bräuchle C. & Hampp N. (1991). Bacteriorhodopsin: a biological material for information processing. *Quart. Rev. Biophys.* **24**, 425–478.
- Ovchinnikov, Yu. A., Abdulaev, N. G., Feigira, M. Y., Kiselev, A. V. & Lobanov, N. A. (1979). The structural basis of the functioning of bacteriorhodopsin: an overview. *FEBS Letters*, **100**, 219–224.
- Plöhn, H.-J. & Büldt, G. (1986). The determination of label positions in membrane proteins by neutron and anomalous X-ray diffraction of powder samples. *J. Appl. Cryst.* **19**, 255–261.
- Popot, J.-L. (1993). Integral membrane protein structure: transmembrane  $\alpha$ -helices as autonomous folding domains. *Curr. Opin. Struct. Biol.* **3**, 532–540.
- Popot, J.-L. & Engelman, D. M. (1990). Membrane protein folding and oligomerization: the two-stage model. *Biochemistry*, **29**, 4031–4037.
- Popot, J.-L., Trehwella, J. & Engelman, D. M. (1986). Reformation of crystalline purple membrane from purified bacteriorhodopsin fragments. *EMBO J.* **5**, 3039–3044.
- Popot, J.-L., Gerchman, S.-E. & Engelman, D. M. (1987). Refolding of bacteriorhodopsin in lipid bilayers: a thermodynamically controlled two-stage process. *J. Mol. Biol.* **198**, 655–676.
- Popot, J.-L., Engelman, D. M., Gurel, O., and Zaccari, G. (1989). Tertiary structure of bacteriorhodopsin: positions and orientations of helices A and B in the structural map determined by neutron diffraction. *J. Mol. Biol.* **210**, 829–847.
- Popot, J.-L., de Vitry, C. & Atteia, A. (1993). Folding and assembly of integral membrane proteins: an introduction. In *Membrane Protein Structure: Experimental Approaches* (White, S. H., ed.), Oxford University Press, Oxford, in the press.
- Reiss-Husson, F. (1992). Crystallization of membrane proteins. In *Crystallization of Nucleic Acids and Proteins. A Practical Approach*. (Ducruix, A. & Giegé, R., eds), pp. 175–193. IRL Press, Oxford.
- Samatey, F. A. (1992). Etude structurale de la bactériorhodopsine et analyse du réseau de la membrane pourpre par diffraction des neutrons. Thèse de Doctorat d'Université, Université Joseph Fourier, Grenoble.
- Schindler, P. A., van Dorsselaer, A. & Falick, A. M. (1993). Analysis of hydrophobic proteins and peptides by electrospray ionization mass spectrometry. *Anal. Biochem.* **213**, 256–263.
- Seiff, F., Westerhausen, J., Wallat, I. & Heyn, M. P. (1986). Location of the cyclohexene ring of the chromophore of bacteriorhodopsin by neutron diffraction with selectively deuterated retinal. *Proc. Nat. Acad. Sci., U.S.A.* **83**, 7746–7750.
- Sklenar, H., Etchebest, C. & Lavery, R. (1989). Describing protein structure: a general algorithm yielding complete helicoidal parameters and a unique overall axis. *Proteins: Struct. Funct. Genet.* **6**, 46–60.
- Sobol, A. G., Arseniev, A. S., Abdulaeva, G. V., Musina, L. Yu. & Bystrov, V. F. (1992). Sequence-specific resonance assignment and secondary structure of (1-71) bacterioopsin. *J. Biomol. NMR*, **2**, 161–171.
- Stern, L. J., Ahl, P. L., Marti, T., Mogi, T., Duñach, M., Berkowitz, S., Rothschild, K. J. & Khorana, H. G. (1989). Substitution of membrane-embedded aspartic acids in bacteriorhodopsin causes specific changes in different steps of the photochemical cycle. *Biochemistry*, **28**, 10035–10042.
- Stoerkenius, W. & Kunau, W. H. (1968). Further characterization of particulate fractions from lysed cell envelopes of *Halobacterium halobium* and isolation of gas vacuole membranes. *J. Cell Biol.* **38**, 337–357.
- Stoerkenius, W. & Rowen, R. (1967). A morphological study of *Halobacterium halobium* and its lysis in media of low salt concentration. *J. Cell Biol.* **34**, 365–393.
- Trehwella, J., Anderson, S., Fox, R., Gogol, E., Khan, S.

- & Zaccāi, G. (1983). Assignment of segments of bacteriorhodopsin sequence to position in the structural map. *Biophys. J.* **42**, 233–241.
- Tufféry, P., Etchebest, C., Hazout, S. & Lavery, R. (1991). A new approach to the rapid determination of protein side-chain conformations. *J. Biomol. Struct. Dynam.* **8**, 1267–1289.
- Tufféry, P., Etchebest, C., Popot, J.-L. & Lavery, R. (1994). Prediction of the positioning of the seven transmembrane  $\alpha$ -helices of bacteriorhodopsin. A molecular simulation study. *J. Mol. Biol.* **236**, 1105–1122.
- Unwin, P. N. T. & Henderson, R. (1975). Molecular structure determination by electron microscopy of unstained crystalline specimens. *J. Mol. Biol.* **94**, 425–440.
- Zaccāi, G. (1987). Structure and hydration of purple membrane in different conditions. *J. Mol. Biol.* **194**, 569–572.
- Zaccāi, G. & Gilmore, D. J. (1979). Areas of hydration in the purple membrane of *Halobacterium halobium*: A neutron diffraction study. *J. Mol. Biol.* **132**, 181–191.

*Edited by A. Klug*

*(Received 2 September 1993; accepted 17 November 1993)*